Chiral anomaly and nonlinear magnetotransport in time reversal symmetric Weyl semimetals

Debottam Mandal,* Kamal Das,† and Amit Agarwal‡
Department of Physics, Indian Institute of Technology Kanpur, 208016 Kanpur, India

(Received 21 January 2022; revised 24 June 2022; accepted 6 July 2022; published 26 July 2022)

The recent discovery of the quantum nonlinear Hall effect has revived the field of nonlinear transport. Here, we investigate the magnetic-field-induced nonlinear transport in time reversal symmetric Weyl semimetals. We show that the interplay of the band-geometric quantities, such as the Berry curvature, and the magnetic part of the Lorentz force can give rise to finite nonlinear Hall conductivity that is linear in the magnetic field. In addition, we show that the chiral chemical potential which represents chiral anomaly gives rise to linear magnetic-field-dependent nonlinear longitudinal conductivities along with the nonlinear Hall conductivities. Such nonlinear conductivities can manifest through nonlinear transport measurement as well as nonlinear optical phenomena like photocurrent and the second harmonic generation.

DOI: 10.1103/PhysRevB.106.035423

I. INTRODUCTION

Weyl semimetals (WSM) are well known for hosting low-energy quasiparticle excitation which mimics the properties of Weyl fermions [1–8]. Their novel bulk electronic structure comprises of doubly degenerate linear band crossing of non-degenerate bands, known as Weyl nodes. In addition, these materials support nontrivial and exotic Fermi arc states on their surface. Intense research focused on the impact of Weyl quasiparticles on physical properties has led to the discovery of several novel bulk phenomena [9–11] such as the quantum anomalies [12], and some unconventional surface phenomena [13,14]. Many of the bulk properties of WSM can be understood in terms of the Berry curvature associated with Weyl nodes, which act as source and sink of Berry curvature depending on the chirality of the nodes. The Weyl semimetal phase with space inversion symmetry (SIS) is realized in some magnetic systems [1,15,16], and it can also be induced in Dirac semimetals such as Cd_3As_2 [17] and Na_3Bi [18] by a magnetic field. Weyl systems with time reversal symmetry (TRS) have been realized in the TaAs family [2–4,19], amongst others. In addition to these, WSM where both the symmetries are broken [20] have been recently realized in *R*AlGe family (R = rare earth) [21] and in CeAlSi [22].

The realization of WSM in SIS broken materials has further promoted the exploration of second-order nonlinear (NL) responses [23–25] in them. It has been shown that due to its topological aspects, the photogalvanic responses [26–33] and the second harmonic generation [34] show novel behavior in WSM. Furthermore, the recently discovered Berry curvature dipole-induced NL anomalous Hall effect [35–40] has also been realized in WSM [41–43] in the absence of any magnetic field. Owing to these, it is expected that the NL responses of WSM in the presence of a magnetic field will also incorporate rich physics [44–46]. In the strong magnetic field limit, the NL conductivities have been found to show quantum oscillation behavior [28,30] owing to the presence of Landau levels, while the Berry curvature induced corrections in the semiclassical equations of motion [47] have been shown to give rise to nontrivial responses in the weak magnetic field regime [44,45,48–52].

In this paper, we explore the magnetic-field-induced NL transport coefficients in WSM with TRS. This is quantified through the NL conductivities σ_{abc} defined from the relation $j_{2,a} = \sigma_{abc}E_bE_c$, where $j_{2,a}$ is the current and $E_b(E_c)$ are the electric field. Using the semiclassical Boltzmann transport formalism in the weak magnetic field regime, we show that the SIS broken WSM possesses NL conductivities both in longitudinal and Hall directions that vary linearly with the magnetic field. We show that the physical origin of the NL conductivities can be attributed to two different physical mechanisms. The first mechanism arises from the interplay between the band geometry and the magnetic field component of the Lorentz force. The other mechanism is dependent on the chiral chemical potential, which arises from the chiral anomaly in WSMs semimetals.

More specifically, we show that in the chiral chemical potential independent conductivity, the NL Hall conductivity with the same last two indices can be expressed as $\sigma_{abb}(a \neq b) \propto B_a$, and the Hall conductivities are finite only when a and b are cyclic coordinates. Such NL Hall conductivity (perpendicular to the applied electric field) drives current along the direction of the magnetic field. The physical mechanisms responsible for this are the Lorentz force, the Berry curvature dependent correction to the phase-space factor, and the Berry curvature induced magnetic velocity correction. Furthermore, the NL Hall conductivity with the different last two indices can be expressed as $\sigma_{aab}(a \neq b) \propto B_b$. For such NL conductivities current flows perpendicular to the direction of the magnetic field. The mechanisms behind this contribution are the Lorentz force, correction to the phase-space factor, and

*dmandal@iitk.ac.in
†kamaldas@iitk.ac.in
‡amitag@iitk.ac.in

the "Berry force." In the chiral chemical potential dependent sector, the internode scattering between the opposite chirality nodes gives rise to NL longitudinal and NL Hall conductivities that are linear in the magnetic field. These contributions are related to the chiral anomaly in WSMs semimetals, which is a well-known phenomenon. Since these contributions are proportional to the internode scattering timescale (τ_v), they are expected to play pivotal roles in the chiral limit where $\tau_v \gg \tau$. These novel NL Hall conductivities can be measured through NL resistivity measurements in magnetotransport experiments [53–56]. In addition, they can also manifest through nonlinear optical experiment of photocurrent and second harmonic generation.

The rest of the paper is organized as follows: In Sec. II we discuss the semiclassical Boltzmann transport formalism and derive the generic forms of the NL conductivities. We present our model-specific calculations of the NL conductivities for the inversion symmetry broken WSM in Sec. III. This is followed by a discussion in Sec. IV and, finally, we summarize our results in Sec. V.

II. SEMICLASSICAL THEORY FOR NONLINEAR CONDUCTIVITIES

In this section, we present the general expressions of second-order NL conductivities in quantum materials in presence of a magnetic field. For an ac electric field, two different NL conductivities are commonly defined. The second harmonic conductivity relates the applied electric field to the second harmonic current $[\boldsymbol{j}_2^{(2\omega)}]$ via the phenomenological relation $j_{2,a}^{(2\omega)} = \sigma_{abc} E_b E_c$. Here, sum over the repeated spatial indices (a, b, c) is implied. The dc or rectification NL conductivity (σ^R_{abc}) relates the rectification current $[\boldsymbol{j}_2^{(0)}]$ to the applied electric field through $j_{2,a}^{(0)} = \sigma^R_{abc} E_b E_c^*$. In this work we primarily focus on the second harmonic conductivity.

To calculate the NL current, we employ the semiclassical Boltzmann transport formalism. In this formalism, the electrical current is expressed as $\boldsymbol{j} = -e\int [d\boldsymbol{k}] D^{-1} \dot{\boldsymbol{r}} g(t)$, where "$-e$" is the electronic charge and $[d\boldsymbol{k}] = d\boldsymbol{k}/(2\pi)^3$. It is evident from the above expression that we need three key ingredients for calculating the current. These are (i) the equations of motion of the carriers, (ii) the phase-space density D^{-1}, and, (iii) the nonequilibrium distribution function (NDF) $g(t)$.

In presence of a homogeneous time-dependent electric field $\boldsymbol{E}(t)$ and a static magnetic field $\boldsymbol{B}$, the equations of motion of the charge carriers, in a given band, are given by [57–60]

$$\dot{\boldsymbol{r}} = D\Big[\tilde{\boldsymbol{v}} + \frac{e}{\hbar}\boldsymbol{E}\times\boldsymbol{\Omega} + \eta\frac{e}{\hbar}(\tilde{\boldsymbol{v}}\cdot\boldsymbol{\Omega})\boldsymbol{B}\Big], \tag{1}$$

$$\hbar\dot{\boldsymbol{k}} = D\Big[-e\boldsymbol{E} - \alpha e(\tilde{\boldsymbol{v}}\times\boldsymbol{B}) - \zeta\frac{e^2}{\hbar}(\boldsymbol{E}\cdot\boldsymbol{B})\boldsymbol{\Omega}\Big]. \tag{2}$$

Here, $1/D = [1 + \gamma\frac{e}{\hbar}\boldsymbol{B}\cdot\boldsymbol{\Omega}]$ is the phase-space factor and $\boldsymbol{\Omega} = \boldsymbol{\nabla}_{\boldsymbol{k}}\times\langle u|i\boldsymbol{\nabla}_{\boldsymbol{k}}|u\rangle$ is the Berry curvature with $|u\rangle$ being the periodic part of the Bloch wave function. The band velocity, modified by the orbital magnetic moment (OMM) $\boldsymbol{m}$, is given by $\tilde{\boldsymbol{v}} = \boldsymbol{v} - \boldsymbol{v}_{\rm m}$ where we have defined $\hbar\boldsymbol{v} = \partial\epsilon/\partial\boldsymbol{k}$ and $\hbar\boldsymbol{v}_{\rm m} = \partial\epsilon_{\rm m}/\partial\boldsymbol{k}$ with $\epsilon_{\rm m} = \boldsymbol{m}\cdot\boldsymbol{B}$. Note that the magnetic field modifies the band energy as $\tilde{\epsilon} = \epsilon - \xi\epsilon_{\rm m}$, through the Zeeman-type coupling of the magnetic field and the OMM, $\boldsymbol{m} = -i\frac{e}{2\hbar}\langle\boldsymbol{\nabla}_{\boldsymbol{k}}u|\times(\hat{H}-\epsilon)|\boldsymbol{\nabla}_{\boldsymbol{k}}u\rangle$. We emphasize that to keep track of the sources of various magnetic field dependencies, we explicitly put α for the magnetic part of the Lorentz force, ζ for the Berry force, η for the magnetic velocity, γ for the phase-space factor, and ξ for the OMM. At the end of the calculation, all these "tracking" factors will be set to 1.

The NDF is calculated from the iterative solution of the Boltzmann equation. Below we solve the Boltzmann transport equation within the relaxation time approximation using the two scattering time approaches and study its consequences on the nonlinear transport coefficients. In the steady state, we have the Boltzmann equation for each Weyl node of the form [61]

$$\frac{\partial g}{\partial t} + \dot{\boldsymbol{k}}\cdot\boldsymbol{\nabla}_{\boldsymbol{k}} g = -\frac{g-\bar{g}}{\tau} - \frac{\bar{g}-\tilde{f}}{\tau_v}. \tag{3}$$

Here, g, $\bar{g}$, and $\tilde{f}$ are the nonequilibrium local distribution, local equilibrium distribution (for each node), and the global equilibrium distribution function, respectively. The OMM and the magnetic field Zeeman coupling induced global equilibrium distribution function are given as $\tilde{f} = f(\epsilon - \xi\boldsymbol{m}\cdot\boldsymbol{B})$ with $f(\epsilon) = 1/[1 + e^{(\epsilon-\mu)/k_BT}]$ being the Fermi-Dirac distribution function at chemical potential μ and temperature T, with k_B being the Boltzmann constant. In Eq. (3), the first term on the right-hand side represents the effect of intranode scattering with scattering timescale τ, and the second term represents the internode scattering that relaxes the local equilibrium distribution function to the global equilibrium distribution function with effective relaxation time τ_v.

In the weak electric field limit, the nonequilibrium part of the distribution function can be written as a power series of electric-field-dependent terms: $\sum_{n=1}^{\infty} f_n$ where $f_n \propto E^n$. We restrict ourselves up to f_2 for the calculation of second-order NL response. The calculation of linear order distribution functions including the effect of chiral anomaly in terms of chiral chemical potential $\delta\mu$ is well known and presented in Appendix A. Here, we will focus on the second-order nonlinear distribution function, especially on the effect of chiral anomaly. For ac electric field, we consider the ansatz [35,62]

$$f_2(t) = f_2^{(0)} + f_2^{(0)*} + f_2^{(2\omega)}e^{i2\omega t} + f_2^{(2\omega)*}e^{-i2\omega t}, \tag{4}$$

where $f_2^{(0)}$ represents the dc (or rectification) part and $f_2^{(2\omega)}$ represents the second harmonic part of the NL distribution function. With this, we construct the Boltzmann equation for $f_2^{(2\omega)}$ which is given by

$$\begin{aligned} i2\omega f_2^{(2\omega)} - \frac{D}{\hbar}\Big[e\boldsymbol{E} + \zeta\frac{e^2}{\hbar}(\boldsymbol{E}\cdot\boldsymbol{B})\boldsymbol{\Omega}\Big]\cdot\boldsymbol{\nabla}_{\boldsymbol{k}} f_1^{(\omega)} \\ - \frac{D}{\hbar}\alpha e(\boldsymbol{v}\times\boldsymbol{B})\cdot\boldsymbol{\nabla}_{\boldsymbol{k}} f_2^{(2\omega)} \\ = -\frac{f_2^{(2\omega)}}{\tau} + \Big(1 - \frac{\tau}{\tau_v}\Big)\frac{\bar{f}_2^{(2\omega)}}{\tau}. \end{aligned} \tag{5}$$

Here, $\bar{f}_2^{(2\omega)} = \bar{g}_2^{(2\omega)} - \tilde{f}$ and $f_1^{(\omega)}$ is the first order in electric field contribution of the NDF (see Appendix A for more details). Since the deviation of the NL distribution function from the equilibrium distribution is expected to contain both first-

and second-order derivatives of the Fermi function, we can express $\bar{f}_2 = \delta\mu^{(21)} f' + \delta\mu^{(22)} f''$, with $f' = \partial_\epsilon f$ and $f'' = \partial_\epsilon^2 f$. Here, $\bar{f}_2$ is the dc counterpart of the deviation of the local distribution function. It has been shown that the number of carriers do not change in the second order in electric field [51,63]. Consequently, we consider $\bar{f}_2 = 0$. Therefore, the nonequilibrium distribution function second order in electric field is given by

$$f_2^{(2\omega)} = \sum_\nu \left(\alpha D \tau_{2\omega} \hat{L}\right)^\nu \left[D \frac{e\tau_{2\omega}}{\hbar}\left(\boldsymbol{E} + \zeta \frac{e}{\hbar}(\boldsymbol{E}\cdot\boldsymbol{B})\boldsymbol{\Omega}\right)\cdot \boldsymbol{\nabla}_{\boldsymbol{k}} f_1^{(\omega)}\right]. \tag{6}$$

In Eq. (6), we have defined $\hat{L} = \frac{e}{\hbar}(\boldsymbol{v}\times\boldsymbol{B})\cdot\boldsymbol{\nabla}_{\boldsymbol{k}}$ as the Lorentz force (magnetic part) operator. The modified scattering times are defined as $\tau_\omega = \tau/(1+i\omega\tau)$ and $\tau_{2\omega} = \tau/(1+i2\omega\tau)$. It is straightforward to expand the master solution (6) and obtain the distribution function up to any order of magnetic field dependence. In this paper we are interested in the lowest (linear) order of magnetic field dependence and the key steps of the calculation have been highlighted in Appendix B. Note that from Eq. (6) we can construct the rectification part of the distribution function $f_2^{(0)}$ by substituting $\tau_{2\omega} \to \tau$ and $\boldsymbol{E} \to \boldsymbol{E}^*$.

From the general expression of Eq. (6) it is evident that the nonlinear distribution function will have two parts of separate origin. They stem from the two parts of the linear distribution function which we denote as $\langle f_1^\omega\rangle$, the part that is independent of the chiral chemical potential and $\langle\langle f_1^\omega\rangle\rangle$ for the part that is dependent on chiral chemical potential (see Appendix A for details of the calculations). To be specific about these different parts in the nonlinear distribution function, we use single angular brackets $\langle f_2^{2\omega}\rangle$ to denote the part that is independent of the chiral chemical potential and double angular brackets $\langle\langle f_2^{2\omega}\rangle\rangle$ for the part that is proportional to the chiral chemical potential. In the following subsections, we calculate the NL conductivities originating from these two parts of the distribution function, separately.

A. Conductivities independent of chiral chemical potential

In this section, using the NDF independent of chiral chemical potential, we calculate the NL conductivities. We emphasize that in addition to the second-order NL distribution function, the NL current can also arise from the linear-$\boldsymbol{E}$ part of the distribution function when it is combined with the anomalous velocity $\boldsymbol{E}\times\boldsymbol{\Omega}$. The NL conductivities can be expressed in the form of a momentum-dependent conductivity $\tilde{\sigma}_{abc}$, where $\sigma_{abc} = -e^3\tau_\omega/\hbar\int[d\boldsymbol{k}]\tilde{\sigma}_{abc}$. The magnetic-field-independent part of the NL conductivity is obtained to be

$$\tilde{\sigma}^{(0)}_{abc} = \varepsilon_{abd}\Omega_d v_c f' + \tau_{2\omega} v_a \partial_b v_c f'. \tag{7}$$

Here, ε_{abd} is the antisymmetric Levi-Civita symbol. The first term of Eq. (7) is the NL anomalous Hall conductivity [37] and the second term is the NL Drude conductivity. The expression of magnetic-field-dependent part of the NL conductivity is a bit more complicated as various magnetic field contributions come into play. The total NL conductivity (linear in the magnetic field) can be expressed as $\tilde{\sigma}^{(1)}_{abc} = \tilde{\sigma}^{(\eta)}_{abc} + \tilde{\sigma}^{(\zeta)}_{abc} + \tilde{\sigma}^{(\alpha)}_{abc} + \tilde{\sigma}^{(\gamma)}_{abc} + \tilde{\sigma}^{(\xi)}_{abc}$. The different contributions to the magnetoconductivity can be calculated to be

$$\tilde{\sigma}^{(\eta)}_{abc} = \tau_{2\omega}\Omega_{\rm v} B_a \partial_b v_c f', \tag{8}$$

$$\tilde{\sigma}^{(\zeta)}_{abc} = \varepsilon_{abd}\Omega_d\Omega_{\rm v} B_c f' + \tau_{2\omega} v_a(\Omega^{db}_{\rm B}\partial_d v_c + B_c\partial_b\Omega_{\rm v}) f', \tag{9}$$

$$\tilde{\sigma}^{(\alpha)}_{abc} = \tau_\omega \varepsilon_{abd}\Omega_d \hat{L} v_c f' + v_a\left(\tau_{2\omega}^2\hat{L}\partial_b + \tau_\omega\tau_{2\omega}\partial_b\hat{L}\right)v_c f', \tag{10}$$

$$\tilde{\sigma}^{(\gamma)}_{abc} = -\varepsilon_{abd}\Omega_d\Omega_{\rm B} v_c f' - \tau_{2\omega} v_a(\Omega_{\rm B}\partial_b + \partial_b\Omega_{\rm B}) v_c f', \tag{11}$$

$$\tilde{\sigma}^{(\xi)}_{abc} = -\varepsilon_{abd}\Omega_d(v_{{\rm m}c} f' + \epsilon_{\rm m} v_c f'') - \tau_{2\omega} v_{{\rm m}a}\partial_b v_c f' - \tau_{2\omega} v_a \partial_b(v_{{\rm m}c} f' + \epsilon_{\rm m} v_c f''). \tag{12}$$

Here, we have defined $\Omega^{db}_{\rm B} \equiv (e/\hbar)\Omega_d B_b$ and $\Omega_{\rm v} \equiv (e/\hbar)\boldsymbol{\Omega}\cdot\boldsymbol{v}$. We emphasize here that the derivative operator $\partial_b = \partial/\partial k_b$ and $\hat{L}$ operate on all the terms appearing to their right-hand side. Together, Eqs. (8)–(12) describe all the NL conductivity components, which vary linearly with the magnetic field.

In materials that preserve SIS, the energy dispersion, Berry curvature, and the OMM are even functions of the crystal momentum. Consequently, the orbital magnetic moment coupling energy and the corresponding velocity satisfy $\epsilon_{\rm m}(-\boldsymbol{k}) = \epsilon_{\rm m}(\boldsymbol{k})$ and $\boldsymbol{v}_{\rm m}(-\boldsymbol{k}) = -\boldsymbol{v}_{\rm m}(\boldsymbol{k})$, respectively, and the bare band velocity obeys $\boldsymbol{v}(-\boldsymbol{k}) = -\boldsymbol{v}(\boldsymbol{k})$. Using these conditions, it is straightforward to show that all the NL conductivities [Eqs. (7)–(12)] vanish in presence of SIS, as expected. If the SIS is broken, the presence or absence of TRS affects the NL conductivity. In presence of TRS, while the energy dispersion is an even function, the Berry curvature and the OMM are odd functions of the crystal momentum. Consequently, we have $\epsilon_{\rm m}(-\boldsymbol{k}) = -\epsilon_{\rm m}(\boldsymbol{k})$, $\boldsymbol{v}_{\rm m}(-\boldsymbol{k}) = \boldsymbol{v}_{\rm m}(\boldsymbol{k})$, and $\boldsymbol{v}(-\boldsymbol{k}) = -\boldsymbol{v}(\boldsymbol{k})$. Within these constraints, we find that for the magnetic-field-independent NL conductivities ($\sigma^{(0)}_{abc}$), contributions that are quadratic in the scattering time vanish while linear scattering time-dependent contributions are finite. On the other hand, for the linear magnetic-field-dependent NL conductivity ($\sigma^{(1)}_{abc}$), contributions that are quadratic in scattering time survive while the other (linear and cubic) scattering-time-dependent contributions vanish.

For completeness, and to complement the discussion of the NL conductivity, we also discuss the linear conductivity of WSM (see Appendix A for detailed derivation). The magnetic-field-independent linear conductivity is given by

$$\sigma^{(0)}_{ab} = -e^2\tau_\omega\int[d\boldsymbol{k}] v_a v_b f' - \frac{e^2}{\hbar}\varepsilon_{abc}\int[d\boldsymbol{k}]\Omega_c f. \tag{13}$$

Here, the first term is the Drude conductivity and the second term is the intrinsic anomalous Hall conductivity which vanishes in TRS invariant systems. The linear order in magnetic field contribution to the linear conductivity is given by

$$\sigma^{(1)}_{ab} = -e^2\tau_\omega\int[d\boldsymbol{k}]\big[\big(\eta\Omega_{\rm v} B_a v_b + \alpha\tau_\omega v_a\hat{L} v_b - \gamma v_a\Omega_{\rm B} v_b + \zeta v_a\Omega_{\rm v} B_b\big) f' - \xi\big\{\big(v_{{\rm m}a} v_b + \hbar^{-1}\tau_\omega^{-1}\varepsilon_{abd}\Omega_d\epsilon_{\rm m} + v_a v_{{\rm m}b}\big) f' + v_a\epsilon_{\rm m} v_b f''\big\}\big]. \tag{14}$$

It can be easily checked that in a TRS invariant system, the diagonal components ($a = b$) of Eq. (14) will vanish, consistent with Onsager's relation. So we can only have the linear-$\boldsymbol{B}$-dependent Hall components ($a \neq b$). Furthermore, we find that in presence of TRS only those contributions to the linear-$\boldsymbol{B}$ conductivity are nonzero which are quadratic and zeroth order in the scattering time. From Eq. (14) it is evident that the quadratic dependence of scattering time is described by the Lorentz force and the scattering time-independent contribution has its origin in the OMM [64].

The framework presented in this section for exploring the NL magnetoconductivity is very general, and applicable to all SIS broken materials. In the rest of the paper, we apply this to explore the NL magnetoconductivity in time reversal symmetric WSM.

B. Conductivities originating from chiral chemical potential

In this section, we calculate the nonlinear conductivities that originate from the chiral chemical potential dependent terms of the distribution function, namely, $\langle\langle f_1^{(\omega)}\rangle\rangle$ and $\langle\langle f_2^{(2\omega)}\rangle\rangle$. First, we focus on the linear order distribution function. Since $\langle\langle f_1^{(\omega)}\rangle\rangle$ is linear in electric field, only the anomalous velocity (electric field dependent) can induce a nonlinear current that is linear in magnetic field. For each Weyl node, this current is given by

$$\boldsymbol{j}_2 = \frac{e^2}{\hbar}\int [d\boldsymbol{k}](\boldsymbol{E}\times\boldsymbol{\Omega})\frac{\tau_\omega}{\tau}\Big(1-\frac{\tau}{\tau_v}\Big)\delta\mu f'. \tag{15}$$

Here, $\delta\mu = s\tau_v\frac{e^2\hbar v_F^3}{2\mu^2}\boldsymbol{E}\cdot\boldsymbol{B}$, with s as the chirality of the Weyl node [65]. Now, in presence of TRS the Berry curvature satisfies $\boldsymbol{\Omega}(-\boldsymbol{k}) = -\boldsymbol{\Omega}(\boldsymbol{k})$, and hence the NL conductivity originating from Eq. (15) vanishes identically. Consequently, we remark that the chiral anomaly induced NL Hall effect mentioned in Ref. [52] vanishes in our system due to the presence of TRS.

We now focus on the second-order NL distribution function. To obtain the NL distribution function from Eq. (6) proportional to the chiral chemical potential $\delta\mu$, which is linear in the magnetic field, we have ignored the Lorentz force operator and the phase-space density. This is reasonable as we are only interested in the linear magnetic field dependence. Additionally, we also ignore the Berry force term, and obtain the NL distribution function as

$$\langle\langle f_2^{(2\omega)}\rangle\rangle = -\frac{e\tau_{2\omega}}{\hbar}\frac{\tau_\omega}{\tau}\Big(1-\frac{\tau}{\tau_v}\Big)\boldsymbol{E}\cdot\nabla_{\boldsymbol{k}}\delta\mu f'. \tag{16}$$

Using this, and noting that only band velocity will contribute to the second-order NL current, we can express the NL chiral anomaly induced conductivity as

$$\sigma_{abc}^{\delta\mu} = s\frac{e^4\tau_\omega\tau_{2\omega}\tau_v\hbar v_F^3}{2\tau\mu^2}\Big(1-\frac{\tau}{\tau_v}\Big)B_c v_a v_b f''. \tag{17}$$

In contrast to Eq. (15), Eq. (17) is expected to be finite in a time reversal symmetric system. We emphasize that in WSMs semimetals where both the symmetries are broken, chiral anomaly contributes to the NL conductivity through both Eqs. (15) and (17). However, there are a couple of subtle differences between the two. First, we note that while the contribution in Eq. (15) is odd ($\propto\tau_v$) in scattering time, the contribution in Eq. (17) is even in scattering time. Second, while Eq. (15) contributes only to the NL Hall conductivities, Eq. (17) manifests through both the NL longitudinal and NL Hall conductivities.

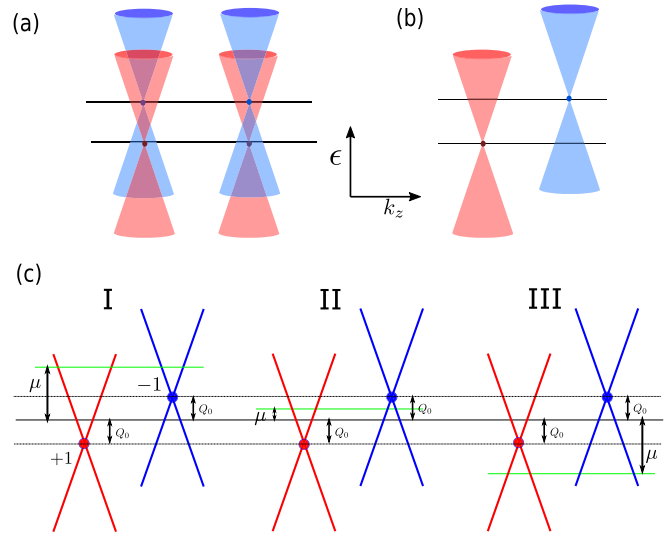

FIG. 1. A schematic depiction of the band dispersion for (a) TRS preserving (with SIS broken) WSM, and (b) TRS broken (with SIS preserved) WSM. Due to the presence of TRS, minimum four Weyl nodes are required in the SIS broken WSM. In contrast, when TRS is absent and SIS is present, a minimum two Weyl nodes is possible. (c) Shows three different scenarios for the location of the Fermi level, with respect to the location of the Weyl points. In the left panel, Fermi level is in the conduction band of both Weyl nodes ($\mu > Q_0 > 0$). In the middle panel, Fermi energy lies in the conduction band of one Weyl node and the valence band of the other Weyl node ($Q_0 > \mu > -Q_0$). The right panel shows the scenario when the Fermi level lies in the valence band of both the Weyl nodes ($\mu < -Q_0 < 0$).

III. NONLINEAR CONDUCTIVITY IN WEYL SEMIMETALS

In this section, we calculate the linear and NL magnetoconductivity for a SIS broken WSM. The simultaneous presence of TRS and SIS forces all the bands in the given material to be doubly degenerate, and this excludes the possibility of the formation of a WSM, in which two nondegenerate linearly dispersing bands cross each other [8]. Thus, for realizing a WSM state, either SIS or TRS or both the symmetries must be broken. In a TRS preserving (SIS broken) WSM, a minimum of four Weyl nodes [66–68] have to be there. Among the four nodes, the nodes with the same chirality are connected by a time reversal invariant momentum, and corresponding charge neutrality points reside at the same energy. However, there is no symmetry restriction among the nodes with different chirality. On the other hand, in a SIS preserving (TRS broken) WSM, a minimum of a single pair of two Weyl nodes of opposite chirality is allowed, and for each such pair of Weyl nodes, the corresponding charge neutrality point resides at different energies. Both of these scenarios have been sketched in Figs. 1(a) and 1(b), respectively. In our work, we present the NL conductivity calculation for a TRS invariant WSM with a minimum of four Weyl nodes as shown in Fig. 1(a).

TABLE I. Symmetrized nonlinear conductivity $\bar{\sigma}_{abc}$, in the units of $\tilde{\sigma}_{\rm NL}$ which is defined in Eq. (20), for the TRS invariant WSM. Here the conductivities are independent of the chiral chemical potential. The subscript a denotes the direction of current flow, and b and c represent the direction of the electric field. The Greek indices in the parentheses denote the sources of the magnetic field that are inducing finite conductivity and the total is obtained by adding all the contributions. The diagonal components of the NL conductivity are identically zero. The NL Hall conductivities with the same last two indices (σ_{abb}) are nonzero when a and b are cyclic coordinates and the magnetic field dependence is dictated by B_a. The Hall conductivities with different last two indices can be written as $\bar{\sigma}_{aab} = \bar{\sigma}_{aba}$ and its magnetic field dependence is determined by B_b.

$\bar{\sigma}_{abc}$	$\bar{\sigma}_{axx}$	$\bar{\sigma}_{ayy}$	$\bar{\sigma}_{azz}$	$\bar{\sigma}_{axy}$	$\bar{\sigma}_{ayz}$	$\bar{\sigma}_{azx}$
$\bar{\sigma}_{xbc}$	0	$B_x(2\eta+\alpha-\gamma)$	0	$-B_y\left(\frac{\alpha}{2}-\frac{\gamma}{2}+\zeta\right)$	0	0
$\bar{\sigma}_{ybc}$	0	0	$B_y(2\eta+\alpha-\gamma)$	0	$-B_z\left(\frac{\alpha}{2}-\frac{\gamma}{2}+\zeta\right)$	0
$\bar{\sigma}_{zbc}$	$B_z(2\eta+\alpha-\gamma)$	0	0	0	0	$-B_x\left(\frac{\alpha}{2}-\frac{\gamma}{2}+\zeta\right)$

The low-energy Hamiltonian of a single Weyl node can be written as [20,69–72]

$$H_s(\boldsymbol{k}) = s\hbar v_F \boldsymbol{\sigma}\cdot(\boldsymbol{k}-s\boldsymbol{Q}) - sQ_0. \tag{18}$$

Here, $\boldsymbol{k}$ is the crystal momentum, $\boldsymbol{\sigma} = (\sigma_x, \sigma_y, \sigma_z)$ are the Pauli matrices, v_F is the Fermi velocity, and $s = \pm 1$ is the chirality index. In Eq. (18), the $\boldsymbol{Q}$ and Q_0 denote the position of the Weyl nodes in the momentum and energy, respectively. For simplicity of calculation, we consider the case where the Weyl node is situated at the origin and emphasize that nonzero $\boldsymbol{Q}$, which breaks the TRS, does not alter any of the results. With $\boldsymbol{Q} = 0$, the Hamiltonian in Eq. (18) simplifies to $H_s(\boldsymbol{k}) = s\hbar v_F \boldsymbol{\sigma}\cdot\boldsymbol{k} - sQ_0$. The breaking of SIS in this model is reflected through the finite Q_0 which positions the Weyl nodes of opposite chirality at different energy. More specifically, the Weyl point of the positive chirality node lies at energy $-Q_0$, while the Weyl point for the negative chirality node lies at Q_0, making the energy separation between the two Weyl nodes equal to $2Q_0$. On the other hand, the TRS is enforced here by considering a minimum of four Weyl nodes in such a way that the two nodes of the same chirality out of the four are situated at the same energy [see Fig. 1(a)]. The energy dispersion and band velocity for the Hamiltonian are given by $\epsilon_s(\boldsymbol{k}) = s_{\rm b}\hbar v_F k - sQ_0$ and $\boldsymbol{v}(\boldsymbol{k}) = s_{\rm b} v_F \boldsymbol{k}/k$, respectively, where $k = |\boldsymbol{k}|$ and $s_{\rm b} = +1$ (-1) for the conduction (valence) band. We note that nonzero Q_0 makes $\epsilon_+(\boldsymbol{k}) \neq \epsilon_-(\boldsymbol{k})$, implying the breaking of inversion symmetry. The Berry curvature and the OMM for this model are given by [45,52]

$$\boldsymbol{\Omega} = -ss_{\rm b}\frac{\boldsymbol{k}}{2k^3}; \quad \boldsymbol{m} = -{\rm sev}_F\frac{\boldsymbol{k}}{2k^2}, \tag{19}$$

respectively. We note that these band-geometric quantities do not depend on the energy separation (Q_0) of the Weyl points in the corresponding Weyl nodes. In contrast to the Berry curvature, the OMM is independent of the band index. Both these band-geometric quantities are highly concentrated near the Weyl point, as expected. Using these in Eqs. (7)–(12), we calculate the NL conductivity for single scattering time and the symmetrized results $\bar{\sigma}_{abc} = (\sigma_{abc} + \sigma_{acb})/2$ are summarized in Table I. We note that the NL Drude conductivity is identically zero due to the presence of TRS. Furthermore, we find that the NL anomalous Hall conductivity is also zero. Although individual Weyl node possesses finite NL anomalous Hall conductivity, the total response vanishes after summing over the nodes. This happens due to the absence of Berry curvature dipole in this system. In order to realize the NL anomalous response [37], the mirror symmetry has to be broken. This is generally achieved in WSM with tilt or with higher-order (band-bending) terms [37,40,73,74] in the effective Hamiltonian.

Coming to the linear magnetic-field-dependent NL conductivities, all the conductivities and their origin of magnetic field dependencies are explicitly highlighted in Table I. For compactness, the various components of the conductivity are expressed as $\bar{\sigma}_{abc} = \tilde{\sigma}_{\rm NL} B_d(\eta, \alpha, \gamma, \zeta, \xi)$ where B_d is the component of the magnetic field along the $d \in (x, y, z)$ axis, and the total contribution is given by the sum of different magnetic field sources. We have defined

$$\tilde{\sigma}_{\rm NL} = \frac{e^4 v_F^2 \tau^2}{\pi^2\hbar^2|\mu|}\frac{r_0}{3\left(1-r_0^2\right)}, \tag{20}$$

with $r_0 \equiv Q_0/|\mu|$. For simplicity, we have taken $\tau_\omega \to \tau$, $\tau_{2\omega} \to \tau$ in the calculation. We find three key features in the NL conductivities. (i) All the longitudinal NL conductivities (σ_{aaa}) vanish within the linear-$\boldsymbol{B}$ approximation. (ii) We find that the NL Hall components with the same last two indices, which we term as "pure" Hall components, such as $\bar{\sigma}_{zxx}, \bar{\sigma}_{yzz}, \bar{\sigma}_{xyy}$ are nonzero and determined by the magnetic velocity term (η) in addition to the phase-space factor (γ) and the magnetic part of the Lorentz force (α). These NL conductivities can be expressed as $\sigma_{abb} \propto B_a$ which implies that the currents corresponding to the conductivity flow along the direction of the applied magnetic field. However, these conductivities are only nonzero for elements where a and b are cyclic coordinate. (iii) The NL Hall components with different last two indices, which we term as the "mixed" Hall components, are determined by the Berry force (ζ) in addition to the phase-space factor (γ) and the Lorentz force (α). The magnetic field dependence of the mixed components, $\sigma_{aab} \propto B_b$, implies that the currents corresponding to the conductivity flow perpendicular to the magnetic field direction. These are some of the main findings of our paper in the context of SIS broken WSM. Interestingly, we find that the OMM (ξ) contributions to the NL conductivity are identically zero for the TRS preserving case.

We emphasize here that for the calculation of conductivities for Weyl nodes with opposite chirality separated in energy, three different scenarios based on the position of the Fermi level, as highlighted in Fig. 1(c), are possible. In scenario I, the Fermi level resides in the conduction band of both the Weyl nodes. In scenario II, the Fermi

level resides in the conduction band of one Weyl node and in the valence band of the other Weyl node. In scenario III, the Fermi level resides in the valence band of both the Weyl nodes. Interestingly, we find that the total conductivity, including all the Weyl nodes, can be expressed by same expression for these three scenarios. This has been shown in Appendix C in detail.

Although we have considered the three scenarios, a continuous transition of Fermi level among them is not allowed within our formalism. This is because the employed semiclassical Boltzmann formalism is generally valid at high carrier densities such that $\mu \gg \hbar/\tau$ [75,76]. Hence, the above results are not applicable near the limit $|r_0| = 1$, when the chemical potential is located at the Weyl point of either of the two Weyl nodes.

Now, we compare our results with some recent related works [45,52] and highlight the differences. We note that in Ref. [45] the authors provide result of a single Weyl node. To our satisfaction, we can obtain those results by setting $Q_0 = 0$ in our single-node calculations presented in Appendix C. We emphasize that total NL responses from all nodes are zero for $Q_0 = 0$ as the inversion symmetry is restored. Recently in Ref. [52], it has been shown that the inversion symmetry broken tilted WSM possesses NL magnetoresponse. We note that the NL conductivities discussed in Ref. [52] are linear in scattering time τ; however the NL conductivities we discuss in our paper are proportional to the square of the scattering time τ^2. We emphasize here that the TRS has to be broken in addition to SIS in order to obtain linear-τ-dependent NL magnetoconductivity. Comparing the order of magnitude of NL conductivities discussed in our paper with the results in Ref. [52] we find that for certain parameter values $v_F = 3 \times 10^5$ m/s, $\tau = 10^{-13}$ s, $R_s(\text{tilt}) = 0.5$, $\mu = 20$ meV, and $Q_0 = 10$ meV, the conductivities are of the comparable order: $\sigma(R_s = 0)/\sigma(R_s \neq 0) \sim O(10^1)$, where $\sigma(R_s = 0) = \tilde{\sigma}_{\text{NL}}$ and $\sigma(R_s \neq 0)$ is the NL conductivity in Eq. (11) of [52].

Having discussed the NL conductivities that are independent of the chiral chemical potential, we now turn our focus on the chiral chemical potential induced conductivities. Following Eq. (17), the chiral-anomaly-induced contributions are calculated for the TRS preserved Weyl Hamiltonian as

$$\sigma^{\delta\mu}_{abc} = \tilde{\sigma}_{\text{i}}\tilde{\sigma}_{\text{NL}} B_c \delta_{ab}. \tag{21}$$

Here, we have defined

$$\tilde{\sigma}_{\text{i}} = 2\left(\frac{\tau_v}{\tau} - 1\right)\left(1 - r_0^2\right). \tag{22}$$

All the components of this chiral chemical potential induced conductivity are summarized in Table II. We have calculated for different locations of the Fermi level described in Fig. 1, and found that the NL conductivity is identical in all the three scenarios. We note that these new contributions are finite only in presence of finite Q_0, due to the factor $\tilde{\sigma}_{\text{NL}}$. This is expected since SIS breaking is a necessary criterion for having any second-order nonlinear responses. There are a few interesting facts about these NL conductivities. (i) The chiral chemical potential induces the longitudinal NL response linear in magnetic field, provided that the opposite chirality nodes are situated at different energies. (ii) In the chiral limit where $\tau_v \gg \tau$, $\tilde{\sigma}^{\delta\mu}_{abc}$ predominantly determines the nonlinear conductivities. (iii) For these NL conductivities to be nonzero the $\boldsymbol{E} \cdot \boldsymbol{B}$ must be nonzero, i.e., the external fields are nonorthogonal.

TABLE II. Additional contribution to the symmetrized nonlinear conductivity $\bar{\sigma}^{\delta\mu}_{abc}$ due to chiral chemical potential, for the TRS invariant WSM. The results are in the units of $\tilde{\sigma}_{\text{i}}\tilde{\sigma}_{\text{NL}}$, which are defined in Eqs. (20) and (22). Only the mixed Hall conductivities and the longitudinal components reflect the effect of internode scattering.

$\bar{\sigma}^{\delta\mu}_{abc}$	$\bar{\sigma}^{\delta\mu}_{axx}$	$\bar{\sigma}^{\delta\mu}_{ayy}$	$\bar{\sigma}^{\delta\mu}_{azz}$	$\bar{\sigma}^{\delta\mu}_{axy}$	$\bar{\sigma}^{\delta\mu}_{ayz}$	$\bar{\sigma}^{\delta\mu}_{azx}$
$\bar{\sigma}^{\delta\mu}_{xbc}$	B_x	0	0	B_y	0	B_z
$\bar{\sigma}^{\delta\mu}_{ybc}$	0	B_y	0	B_x	B_z	0
$\bar{\sigma}^{\delta\mu}_{zbc}$	0	0	B_z	0	B_y	B_x

For completeness, we now discuss the linear conductivity of WSM, starting from Eqs. (13) and (14). As expected from the Onsager relations, the magnetic-field-induced part of the longitudinal components are identically zero and the Drude conductivity is obtained to be [71]

$$\sigma_{aa} = \frac{2e^2\tau\mu^2\left(1 + r_0^2\right)}{3\pi^2\hbar^3 v_F}, \tag{23}$$

where $a = (x, y, z)$. The Drude contribution is linear in the scattering time and quadratic in the node separation. The Drude conductivity in Eq. (23) reduces to the known result [65,71] in the limit of zero-energy separation between the Weyl points $Q_0 = 0$. Here, the modification in the Drude conductivity corresponds to the fact that the energy separation between the nodes gives rise to different carrier concentrations at the opposite chirality. The linear Hall conductivity is given by

$$\sigma_{ab} = -\varepsilon_{abc} B_c \frac{e^3 v_F \mu}{6\pi^2\hbar^3}\left(\xi \frac{\hbar^2}{\mu^2\left(1 - r_0^2\right)} + 4\alpha\tau^2\right). \tag{24}$$

We highlight that the Hall conductivity has two components: one is quadratic and the other is zeroth order in the scattering time. While the former extrinsic contribution has its origin in the Lorentz force (term $\propto\alpha$), the latter intrinsic contribution (term $\propto\xi$) originates from the OMM [64].

IV. DISCUSSION

In our paper, we have highlighted the interplay of geometric quantities with the Lorentz force to induce linear magnetic-field-dependent conductivity in time reversal symmetric systems. It is important to mention here that the search for magnetic-field-dependent current, especially the photocurrent, started quite early through the work of Ivchenko *et al.* [77]. It was shown that in gyrotropic systems, unpolarized light can induce a magnetic-field-dependent photocurrent, if one considers Zeeman coupling in the carrier dispersion. Since then, several works have proposed magnetic-field-dependent second-order photocurrent based on different mechanisms. For instances, light-induced electric current caused by asymmetric spin-dependent scattering between Zeeman-splitted bands in gyrotropic symmetry classes has been proposed in Refs. [77–80]. On the other hand, a linear magnetic field dependence in the electrical conductiv-

ity [81,82] or the dc photocurrent [83] was shown to arise in chiral systems, where the distribution of the carriers is odd in the wave vector. A similar kind of magnetic field dependence has also been predicted in mesoscopic systems, taking the electron-electron interaction into account [84].

We would like to add here that the results obtained in this paper using the semiclassical Boltzmann theory are quite general, and can also be derived using the recently developed quantum kinetic formalism [85–88]. We found that the latter formalism reconciles with the semiclassical approach in the single-band limit with some subtle differences. For instance, in the semiclassical formalism, the Berry curvature modifies the phase-space density in presence of magnetic field. On the other hand, this modification in the phase space manifests through the equilibrium density matrix (population) in the quantum kinetic theory, instead of the density of states. However, these subtle differences do not alter the overall expressions of the magnetoconductivities.

V. SUMMARY AND CONCLUSION

To wrap up, in this paper we have investigated the second-order NL conductivity in time reversal symmetric WSM in presence of a weak magnetic field. Starting from the semiclassical Boltzmann transport formalism, we obtain the general expressions of all the NL conductivities, and identify the different physical mechanisms contributing to the magnetic field dependencies. Using the developed framework for NL magnetoconductivity in conjugation with appropriate symmetry analysis, we calculate the NL conductivity in WSM with broken SIS. The calculated linear magnetic-field-dependent NL Hall conductivities represent the overall NL Hall responses since the Berry curvature dipole induced NL anomalous Hall effect vanishes in our system. We highlight that the physical mechanisms of NL conductivities in WSM can be categorized into two classes. In one class, which is chiral chemical potential independent, the interplay of the quantum-geometric Berry curvature and the magnetic part of the Lorentz force plays pivotal role. In this class, we predict two types of new NL Hall effects. In one case, which we term as pure NL Hall effect, the current flows along the direction of the magnetic field, but perpendicular to the applied electric field. In the other case, which we term as the mixed NL Hall effect, the NL current flows perpendicular to the magnetic field direction. In the other class, which is chiral chemical potential dependent, the NL conductivities originate from the effect of chiral anomaly. This physical mechanism gives rise to longitudinal conductivities in addition to the Hall conductivities. These newly predicted NL conductivities in WSM can be probed through NL magnetotransport or through NL magneto-optical experiments.

ACKNOWLEDGMENTS

We acknowledge the Department of Physics, IIT Kanpur, the Science Education and Research Board (SERB), and the Department of Science and Technology (DST), Government of India. We sincerely thank one of the anonymous referees of this manuscript.

APPENDIX A: SEMICLASSICAL THEORY FOR LINEAR CONDUCTIVITIES

In this Appendix, we will calculate current that is linear in $\boldsymbol{E}$ field and linear in $\boldsymbol{B}$ field. We assume that in the steady state, the first-order distribution function oscillates with fundamental frequency with the form [35,45] $f_1(t) = f_1^{(\omega)} e^{i\omega t} + f_1^{(\omega)*} e^{-i\omega t}$. We can construct the Boltzmann equation of the form

$$\begin{aligned} i\omega f_1^{(\omega)} - \frac{D}{\hbar}\left[e\boldsymbol{E} + \zeta\frac{e^2}{\hbar}(\boldsymbol{E}\cdot\boldsymbol{B})\boldsymbol{\Omega}\right]\cdot\boldsymbol{\nabla}_k\tilde{f} \\ - \frac{D}{\hbar}\alpha e(\tilde{\boldsymbol{v}}\times\boldsymbol{B})\cdot\boldsymbol{\nabla}_k f_1^{(\omega)} \\ = -\frac{f_1^{(\omega)}}{\tau} + \left(1-\frac{\tau}{\tau_v}\right)\frac{\bar{g}_1^{(\omega)} - \tilde{f}}{\tau}. \end{aligned} \tag{A1}$$

Now, we assume the following form of the local equilibrium in terms of the chiral chemical potential $\bar{f}_1^{(\omega)} \equiv \bar{g}_1^{(\omega)} - \tilde{f} = -\delta\mu f'$ within the Taylor series expansion. From the above equation, we can calculate the nonequilibrium distribution function as

$$\begin{aligned} f_1^{(\omega)} = \sum_v \left(\alpha D\tau_\omega \hat{L}\right)^v \Big[D\frac{e\tau_\omega}{\hbar}\Big(\boldsymbol{E} + \zeta\frac{e}{\hbar}(\boldsymbol{E}\cdot\boldsymbol{B})\boldsymbol{\Omega}\Big)\cdot\boldsymbol{\nabla}_k\tilde{f} \\ - \frac{\tau_\omega}{\tau}\Big(1-\frac{\tau}{\tau_v}\Big)\delta\mu f'\Big]. \end{aligned} \tag{A2}$$

We can separate the distribution function into two parts: $f_1^{(\omega)} = \langle f_1^{(\omega)}\rangle + \langle\langle f_1^{(\omega)}\rangle\rangle$ where we associate the first term to the intranode contributions and the second part to $\delta\mu$, the chiral chemical potential. Here, we mention a few points about the chiral chemical potential dependent part. The chiral chemical potential is given by $\delta\mu = s\tau_v \frac{e^2\hbar v_F^3}{2\mu^2}\boldsymbol{E}\cdot\boldsymbol{B}$ which is linear in magnetic field. The $\delta\mu$ is proportional to the internode scattering time and when the Lorentz operator operates on the chiral chemical potential part it vanishes identically. So we can denote

$$\langle\langle f_1^{(\omega)}\rangle\rangle = -\frac{\tau_\omega}{\tau}\Big(1-\frac{\tau}{\tau_v}\Big)\delta\mu f'. \tag{A3}$$

The rest of the distribution function is $\langle f_1^{(\omega)}\rangle$ and in the rest of the section we denote it without the angular brackets for simplicity of notation. We expand the series in Eq. (A2) in orders of $\boldsymbol{B}$ field in the limit of small magnetic field [44,47,89]. Using this expansion, the nonequilibrium part can be written as $f_1^{(\omega)} = f_{10}^{(\omega)} + f_{11}^{(\omega)}$, where the first subscript denotes the order of electric field and the second subscript denotes the order of magnetic field. We obtain

$$f_{10}^{(\omega)} = e\tau_\omega \boldsymbol{E}\cdot\boldsymbol{v}f', \tag{A4}$$

$$\begin{aligned} f_{11}^{(\omega)} = e\tau_\omega(\zeta\Omega_{\rm v}\boldsymbol{B} - \gamma\Omega_{\rm B}\boldsymbol{v})\cdot\boldsymbol{E}f' \\ - \xi e\tau_\omega\boldsymbol{E}\cdot(\boldsymbol{v}_{\rm m}f' + \epsilon_{\rm m}\boldsymbol{v}f'') \\ + \alpha e\tau_\omega^2\hat{L}\boldsymbol{v}\cdot\boldsymbol{E}f'. \end{aligned} \tag{A5}$$

We note that these results are consistent with the previous studies [44,45,47,90].

Using the distribution functions we can calculate current. The zeroth order in $\boldsymbol{B}$-field current can be written as $\boldsymbol{j}_{10}(t) =$

$\boldsymbol{j}_{10}^{(\omega)} e^{i\omega t} + \boldsymbol{j}_{10}^{(\omega)*} e^{-i\omega t}$. Separating the different order of scattering time dependence, we obtain

$$\boldsymbol{j}_{10}^{(\omega)}(\tau_\omega^0) = -\frac{e^2}{\hbar}\int [d\boldsymbol{k}](\boldsymbol{E}\times\boldsymbol{\Omega})f, \tag{A6}$$

$$\boldsymbol{j}_{10}^{(\omega)}(\tau_\omega) = -e^2\tau_\omega \int [d\boldsymbol{k}]\boldsymbol{v}(\boldsymbol{E}\cdot\boldsymbol{v})f'. \tag{A7}$$

The first one is the intrinsic anomalous Hall effect where current flows perpendicular to the electric field. Symmetry analysis shows that in presence of TRS, the anomalous Hall effect vanishes. The second one is the ordinary Drude current. The linear order in $\boldsymbol{B}$-field current can be written as $\boldsymbol{j}_{11}(t) = \boldsymbol{j}_{11}^{(\omega)} e^{i\omega t} + \boldsymbol{j}_{11}^{(\omega)*} e^{-i\omega t}$. We emphasize that "equilibrium" distribution function in presence of a magnetic field $\tilde{f} = f - \xi\epsilon_{\rm m} f'$ also contributes to the current in addition to the nonequilibrium parts (A4) and (A5). Now, using these we calculate current in various order in scattering time. The even power of scattering time-dependent current is given by

$$\boldsymbol{j}_{11}^{(\omega)}(\tau_\omega^0) = \frac{e^2}{\hbar}\xi\int [d\boldsymbol{k}](\boldsymbol{E}\times\boldsymbol{\Omega})\epsilon_{\rm m} f', \tag{A8}$$

$$\boldsymbol{j}_{11}^{(\omega)}(\tau_\omega^2) = -e^2\tau_\omega^2\alpha\int [d\boldsymbol{k}]\boldsymbol{v}\hat{L}\boldsymbol{v}\cdot\boldsymbol{E}f'. \tag{A9}$$

Current that is linear order in scattering time is given by

$$\begin{aligned}\boldsymbol{j}_{11}^{(\omega)}(\tau_\omega) = e^2\tau_\omega\int [d\boldsymbol{k}][&\xi\boldsymbol{v}_{\rm m}\boldsymbol{E}\cdot\boldsymbol{v}f' - \eta\boldsymbol{B}\Omega_{\rm v}\boldsymbol{v}\cdot\boldsymbol{E}f'\\ &- \boldsymbol{v}(\zeta\Omega_{\rm v}\boldsymbol{B} - \gamma\Omega_{\rm B}\boldsymbol{v})\cdot\boldsymbol{E}f'\\ &+ \xi\boldsymbol{v}\boldsymbol{E}\cdot(\boldsymbol{v}_{\rm m}f' + \epsilon_{\rm m}\boldsymbol{v}f'')].\end{aligned} \tag{A10}$$

The linear-$\boldsymbol{B}$-dependent currents calculated in Eqs. (A8)–(A10) have been earlier discussed in Refs. [44,45,47,90]. In presence of TRS (broken SIS) various quantities satisfy $(\epsilon_{\rm m}, \boldsymbol{\Omega})(-\boldsymbol{k}) = -(\epsilon_{\rm m}, \boldsymbol{\Omega})(\boldsymbol{k})$, $\boldsymbol{v}(-\boldsymbol{k}) = -\boldsymbol{v}(\boldsymbol{k})$, and $\boldsymbol{v}_{\rm m}(-\boldsymbol{k}) = \boldsymbol{v}_{\rm m}(\boldsymbol{k})$, hence, all the contributions $\propto\tau_\omega$ vanish. However, currents proportional to the even power of scattering time survive, out of which the Lorentz force contribution $\propto\tau_\omega^2$ gives rise to the classical Hall effect [89,91], and the anomalous velocity contribution $\propto\tau_\omega^0$ gives rise to OMM-induced intrinsic Hall effect [64]. On the other hand, in presence of SIS (broken TRS) the various quantities satisfy $(\epsilon_{\rm m}, \boldsymbol{\Omega})(-\boldsymbol{k}) = (\epsilon_{\rm m}, \boldsymbol{\Omega})(\boldsymbol{k})$, $\boldsymbol{v}(-\boldsymbol{k}) = -\boldsymbol{v}(\boldsymbol{k})$, $\boldsymbol{v}_{\rm m}(-\boldsymbol{k}) = -\boldsymbol{v}_{\rm m}(\boldsymbol{k})$, and in that case all the linear-$\boldsymbol{B}$-dependent terms are expected to be nonzero.

APPENDIX B: SEMICLASSICAL THEORY FOR THE NONLINEAR CONDUCTIVITIES

In this Appendix, we calculate current that is NL in the $\boldsymbol{E}$ field. The ansatz for the nonequilibrium part of the distribution function quadratic in $\boldsymbol{E}$ field [35,45] can be written as

$$f_2(t) = f_2^{(0)} + f_2^{(0)*} + f_2^{(2\omega)} e^{i2\omega t} + f_2^{(2\omega)*} e^{-i2\omega t}, \tag{B1}$$

where $f_2^{(0)}$ represents the rectification part and $f_2^{(2\omega)}$ represents the second harmonic part. With this, from Eq. (6) we obtain

$$f_2^{(2\omega)} = \sum_\nu \left(\alpha D\tau_{2\omega}\hat{L}\right)^\nu D\frac{e\tau_{2\omega}}{\hbar}\left[\boldsymbol{E} + \zeta\frac{e}{\hbar}(\boldsymbol{E}\cdot\boldsymbol{B})\boldsymbol{\Omega}\right]\cdot\boldsymbol{\nabla}_{\boldsymbol{k}} f_1^{(\omega)} \tag{B2}$$

and

$$f_2^{(0)} = \sum_\nu \left(\alpha D\tau\hat{L}\right)^\nu D\frac{e\tau}{\hbar}\left[\boldsymbol{E}^* + \zeta\frac{e}{\hbar}(\boldsymbol{E}^*\cdot\boldsymbol{B})\boldsymbol{\Omega}\right]\cdot\boldsymbol{\nabla}_{\boldsymbol{k}} f_1^{(\omega)}. \tag{B3}$$

We emphasize that from Eq. (B2) we can generate Eq. (B3) by $\tau_{2\omega}\to\tau$ and $\boldsymbol{E}\to\boldsymbol{E}^*$. Now it is straightforward to separate out the chiral chemical potential dependent and independent terms. The chiral chemical potential dependent part has been discussed in the main text. Here, we discuss the independent part which is denoted as $\langle f_2^{(2\omega)}\rangle$. For brevity, we denote it as $f_2^{(2\omega)}$ in the rest of this section. From this master solution it is now straightforward to separate out the distribution function in various order in magnetic field as $f_2^{(2\omega)} = f_{20}^{(2\omega)} + f_{21}^{(2\omega)}$. These can be calculated as

$$f_{20}^{(2\omega)}(\tau_{2\omega},\tau_\omega) = \frac{e^2\tau_{2\omega}\tau_\omega}{\hbar}(\boldsymbol{E}\cdot\boldsymbol{\nabla}_{\boldsymbol{k}})\boldsymbol{E}\cdot\boldsymbol{v}f', \tag{B4}$$

$$\begin{aligned}f_{21}^{(2\omega)}(\tau_{2\omega},\tau_\omega) = \frac{e^2\tau_{2\omega}\tau_\omega}{\hbar}\Big[&\zeta\frac{e}{\hbar}(\boldsymbol{E}\cdot\boldsymbol{B})(\boldsymbol{\Omega}\cdot\boldsymbol{\nabla}_{\boldsymbol{k}})\boldsymbol{v}\cdot\boldsymbol{E}f'\\ &- \gamma\Omega_{\rm B}(\boldsymbol{E}\cdot\boldsymbol{\nabla}_{\boldsymbol{k}})\boldsymbol{v}\cdot\boldsymbol{E}f'\\ &+ (\boldsymbol{E}\cdot\boldsymbol{\nabla}_{\boldsymbol{k}})\{(\zeta\Omega_{\rm v}\boldsymbol{B} - \gamma\Omega_{\rm B}\boldsymbol{v})\cdot\boldsymbol{E}f'\\ &- \xi\boldsymbol{E}\cdot(\boldsymbol{v}_{\rm m}f' + \epsilon_{\rm m}\boldsymbol{v}f'')\}\Big],\end{aligned} \tag{B5}$$

$$f_{21}^{(2\omega)}(\tau_{2\omega}^2,\tau_\omega) = \alpha\frac{e^2\tau_{2\omega}^2\tau_\omega}{\hbar}\hat{L}(\boldsymbol{E}\cdot\boldsymbol{\nabla}_{\boldsymbol{k}})\boldsymbol{E}\cdot\boldsymbol{v}f',$$

$$f_{21}^{(2\omega)}(\tau_{2\omega},\tau_\omega^2) = \alpha\frac{e^2\tau_{2\omega}\tau_\omega^2}{\hbar}(\boldsymbol{E}\cdot\boldsymbol{\nabla}_{\boldsymbol{k}})\hat{L}\boldsymbol{v}\cdot\boldsymbol{E}f'. \tag{B6}$$

We note that the first two expressions are $\propto\tau^2$ and the last two expressions are $\propto\tau^3$. We can obtain the rectification part $f_2^{(0)}$ from these expressions just by replacing $\tau_{2\omega}$ by τ and $\boldsymbol{E}$, first one from the left, by $\boldsymbol{E}^*$. These results are consistent with the previous studies [44,45].

The magnetic-field-independent contributions to the current come from the semiclassical band velocity and Berry curvature induced anomalous velocity. The second harmonic current that is zeroth order in magnetic field can be written as $\boldsymbol{j}_{20}(t) = \boldsymbol{j}_{20}^{(2\omega)} e^{i2\omega t} + \boldsymbol{j}_{20}^{(2\omega)*} e^{-i2\omega t}$, where

$$\boldsymbol{j}_{20}^{(2\omega)}(\tau_\omega) = -\frac{e^3\tau_\omega}{\hbar}\int [d\boldsymbol{k}](\boldsymbol{E}\times\boldsymbol{\Omega})\boldsymbol{v}\cdot\boldsymbol{E}f', \tag{B7}$$

$$\boldsymbol{j}_{20}^{(2\omega)}(\tau_\omega,\tau_{2\omega}) = -\frac{e^3\tau_\omega\tau_{2\omega}}{\hbar}\int [d\boldsymbol{k}]\boldsymbol{v}(\boldsymbol{E}\cdot\boldsymbol{\nabla}_{\boldsymbol{k}})\boldsymbol{E}\cdot\boldsymbol{v}f'. \tag{B8}$$

The rectification part can be written as $\boldsymbol{j}_{20} = \boldsymbol{j}_{20} + \boldsymbol{j}_{20}^*$ replacing $\tau_{2\omega}$ by τ and $\boldsymbol{E}$ (first one from the left) by $\boldsymbol{E}^*$ in the above expressions. The $\boldsymbol{j}_{20}^{(2\omega)}(\tau_\omega)$ represents the NL anomalous current [37,55] while the second term is the ordinary NL Drude current originating from the band velocity. In presence of TRS but broken SIS, only the NL anomalous Hall contribution is expected to be nonzero. The breaking of SIS plays the key role in the quadratic NL response, as in the presence of SIS both the contributions vanish identically.

For the linear-$\boldsymbol{B}$ contributions, the second harmonic current can be similarly written as $\boldsymbol{j}_{21}(t) = \boldsymbol{j}_{21}^{(2\omega)} e^{i2\omega t} + \boldsymbol{j}_{21}^{(2\omega)*} e^{-i2\omega t}$. In various orders of scattering time we obtain

$$\boldsymbol{j}_{21}^{(2\omega)}(\tau_\omega) = -\frac{e^3\tau_\omega}{\hbar}\int [d\boldsymbol{k}](\boldsymbol{E}\times\boldsymbol{\Omega})[(\zeta\Omega_{\rm v}\boldsymbol{B} - \gamma\Omega_{\rm B}\boldsymbol{v})\cdot\boldsymbol{E}f' - \xi\boldsymbol{E}\cdot(\boldsymbol{v}_{\rm m}f' + \epsilon_{\rm m}\boldsymbol{v}f'')], \tag{B9}$$

$$\boldsymbol{j}_{21}^{(2\omega)}(\tau_\omega^2) = -\alpha\frac{e^3\tau_\omega^2}{\hbar}\int [d\boldsymbol{k}](\boldsymbol{E}\times\boldsymbol{\Omega})\hat{L}\boldsymbol{v}\cdot\boldsymbol{E}f', \tag{B10}$$

$$\begin{aligned}\boldsymbol{j}_{21}^{(2\omega)}(\tau_\omega, \tau_{2\omega}) &= -\frac{e^3\tau_\omega\tau_{2\omega}}{\hbar}\int [d\boldsymbol{k}](\eta\Omega_{\rm v}\boldsymbol{B} - \xi\boldsymbol{v}_{\rm m})(\boldsymbol{E}\cdot\boldsymbol{\nabla}_{\boldsymbol{k}})\boldsymbol{v}\cdot\boldsymbol{E}f' \\ &- \frac{e^3\tau_\omega\tau_{2\omega}}{\hbar}\int [d\boldsymbol{k}]\boldsymbol{v}\Big[\zeta\frac{e}{\hbar}(\boldsymbol{E}\cdot\boldsymbol{B})(\boldsymbol{\Omega}\cdot\boldsymbol{\nabla}_{\boldsymbol{k}})\boldsymbol{v}\cdot\boldsymbol{E}f' \\ &- \gamma\Omega_{\rm B}(\boldsymbol{E}\cdot\boldsymbol{\nabla}_{\boldsymbol{k}})\boldsymbol{v}\cdot\boldsymbol{E}f' \\ &+ (\boldsymbol{E}\cdot\boldsymbol{\nabla}_{\boldsymbol{k}})[(\zeta\Omega_{\rm v}\boldsymbol{B} - \gamma\Omega_{\rm B}\boldsymbol{v})\cdot\boldsymbol{E}f' \\ &-\xi\boldsymbol{E}\cdot(\boldsymbol{v}_{\rm m}f' + \epsilon_{\rm m}\boldsymbol{v}f'')]\Big],\end{aligned} \tag{B11}$$

$$\begin{aligned}\boldsymbol{j}_{21}^{(2\omega)}(\tau_\omega, \tau_{2\omega}^2) &= -\alpha\frac{e^3\tau_\omega\tau_{2\omega}^2}{\hbar}\int [d\boldsymbol{k}]\boldsymbol{v}\hat{L}(\boldsymbol{E}\cdot\boldsymbol{\nabla}_{\boldsymbol{k}})\boldsymbol{v}\cdot\boldsymbol{E}f',\ \boldsymbol{j}_{21}^{(2\omega)}(\tau_\omega^2, \tau_{2\omega}) \\ &= -\alpha\frac{e^3\tau_{2\omega}\tau_\omega^2}{\hbar}\int [d\boldsymbol{k}]\boldsymbol{v}(\boldsymbol{E}\cdot\boldsymbol{\nabla}_{\boldsymbol{k}})\hat{L}\boldsymbol{v}\cdot\boldsymbol{E}f'.\end{aligned} \tag{B12}$$

The NL conductivities extracted from these expressions are presented in the main text. We note that this general formalism for linear $\boldsymbol{B}$-field dependent NL conductivity has been earlier discussed in Refs. [44,45]. It is straightforward to see that in presence of SIS (TRS broken), all these terms vanish identically. In presence of TRS (broken SIS), however, the current $\propto\tau^2$ survives while the contributions $\propto(\tau, \tau^3)$ vanish identically.

APPENDIX C: DETAILS OF CALCULATION FOR NONLINEAR CONDUCTIVITY IN WSM

In this Appendix, we present the details of our calculation of NL conductivity for a pair of Weyl nodes, of which one is situated at energy Q_0 and the other is situated at energy $-Q_0$. For that, we first calculate the NL conductivities of a single Weyl node with band crossing at zero energy given by $H_s(\boldsymbol{k}) = s\hbar v_F\boldsymbol{\sigma}\cdot\boldsymbol{k}$. Then we modify the Fermi energy dependencies for individual nodes to include the positional shift in the energy. The velocity for this model Hamiltonian is given by $\boldsymbol{v} = s_{\rm b}v_F\boldsymbol{k}/k$, while the Berry curvature and OMM are given by [45,52] $\boldsymbol{\Omega} = -ss_{\rm b}\boldsymbol{k}/(2k^3)$ and $\boldsymbol{m} = -sev_F\boldsymbol{k}/(2k^2)$. The linear Drude conductivities which are diagonal components of the linear conductivity matrix in absence of magnetic field are calculated to be [65]

$$\sigma_{aa} = \frac{e^2\tau\mu^2}{6\pi^2\hbar^3 v_F};\quad a\in(x, y, z). \tag{C1}$$

Equation (C1) does not depend on the chirality of the nodes and whether the Fermi levels reside in the conduction band or valence band. In presence of magnetic field the Onsager's reciprocal relations restrict the longitudinal conductivities to be minimum quadratic order in magnetic field which is out of the scope of this paper. However, the off-diagonal components can have minimum linear-$\boldsymbol{B}$ dependence and are obtained to be [64]

$$\sigma_{ab} = -\varepsilon_{abc}B_c\frac{s_{\rm b}e^3v_F}{24\pi^2\hbar^3|\mu|}(\xi\hbar^2 + 4\alpha\tau^2\mu^2). \tag{C2}$$

Note that the OMM and Lorentz force cause the ordinary Hall effect.

The magnetic-field-independent and linear-$\boldsymbol{B}$-dependent NL conductivities have been summarized in Table III. We obtain the NL anomalous Hall conductivities to be

$$\sigma_{abc}^{\rm NAH} = -\varepsilon_{abc}\frac{se^3\tau}{12\pi^2\hbar^2}. \tag{C3}$$

We note that it is independent of chemical potential and depends on the chirality. So, even for Weyl nodes separated in energy its total contribution will vanish. The magnetic-field-dependent NL conductivities originate from various sources and are written in units of

$$\sigma_{\rm NL}^{\rm S} = ss_{\rm b}\frac{\chi_0}{12}\quad\text{with}\quad\chi_0 = \frac{e^4\tau^2v_F^2}{\pi^2\hbar^2|\mu|}. \tag{C4}$$

The various contributions of magnetic field are also highlighted in the table inside the parentheses. We note that our results for the NL conductivities are consistent with Ref. [45], where the effect of Lorentz force effect was ignored. If we ignore the effect of Lorentz force, then for magnetic field along the $\hat{z}$ the expression of σ_{zxx} matches with the expression given in Ref. [45].

Given the expressions of NL conductivity for a Weyl node at zero energy, now we will show how to modify these expressions to obtain results for Weyl nodes separated in energy. We will show this for Eq. (C4) and the modification in linear conductivities can be obtained following similar steps. For scenario I shown in Fig. 1(c) we obtain

$$\begin{aligned}\sigma_{\rm NL}^{\rm S}(+1) &= \frac{e^4\tau^2v_F^2}{12\pi^2\hbar^2(|\mu| + Q_0)},\ \sigma_{\rm NL}^{\rm S}(-1) \\ &= -\frac{e^4\tau^2v_F^2}{12\pi^2\hbar^2(|\mu| - Q_0)};\end{aligned} \tag{C5}$$

for scenario III we obtain

$$\begin{aligned}\sigma_{\rm NL}^{\rm S}(+1) &= -\frac{e^4\tau^2v_F^2}{12\pi^2\hbar^2(|\mu| - Q_0)},\ \sigma_{\rm NL}^{\rm S}(-1) \\ &= \frac{e^4\tau^2v_F^2}{12\pi^2\hbar^2(|\mu| + Q_0)};\end{aligned} \tag{C6}$$

and for scenario II we obtain

$$\begin{aligned}\sigma_{\rm NL}^{\rm S}(+1) &= \frac{e^4\tau^2v_F^2}{12\pi^2\hbar^2(\pm|\mu| + Q_0)}, \\ \sigma_{\rm NL}^{\rm S}(-1) &= -\frac{e^4\tau^2v_F^2}{12\pi^2\hbar^2(\pm|\mu| - Q_0)}.\end{aligned} \tag{C7}$$

In Eq. (C7) the $+$ $(-)$ sign in the denominator in front of $|\mu|$ corresponds to $\mu > 0$ $(\mu < 0)$ in scenario II. The total NL conductivities are obtained by adding the contribution from

TABLE III. Nonlinear conductivity (not symmetrized) (in units of $ss_b\chi_0/12$) for a single node of a WSM with band crossing (charge neutrality point) situated at zero energy. Here, we have defined $\chi_0 = e^4\tau^2 v_F^2/(\pi^2\hbar^2|\mu|)$ and $\sigma_0 = e^3\tau/(\pi^2\hbar^2)$. Note that we have also included the NL anomalous Hall effect here which is independent of magnetic field.

σ_{abc}	σ_{axx}	σ_{axy}	σ_{axz}	σ_{ayx}	σ_{ayy}	σ_{ayz}	σ_{azx}	σ_{azy}	σ_{azz}
σ_{xbc}	$(-2\eta+2\zeta)B_x$	$(-\gamma+2\zeta)B_y$	$(-\gamma+2\zeta)B_z$	αB_y	$(-2\eta-\alpha+\gamma)B_x$	$-s_b\frac{\sigma_0}{\chi_0}$	$-\alpha B_z$	$-s_b\frac{\sigma_0}{\chi_0}$	$(-2\eta+\alpha+\gamma)B_x$
σ_{ybc}	$(-2\eta+\alpha+\gamma)B_y$	$-\alpha B_x$	$-s_b\frac{\sigma_0}{\chi_0}$	$(-\gamma+2\zeta)B_x$	$(-2\eta+2\zeta)B_y$	$(-\gamma+2\zeta)B_z$	$-s_b\frac{\sigma_0}{\chi_0}$	αB_z	$(-2\eta-\alpha+\gamma)B_y$
σ_{zbc}	$(-2\eta-\alpha+\gamma)B_z$	$-s_b\frac{\sigma_0}{\chi_0}$	αB_x	$-s_b\frac{\sigma_0}{\chi_0}$	$(-2\eta+\alpha+\gamma)B_z$	$-\alpha B_y$	$(-\gamma+2\zeta)B_x$	$(-\gamma+2\zeta)B_y$	$(-2\eta+2\zeta)B_z$

the two nodes. Comparing scenario I with III, one can easily identify that

$$\sigma_{\rm NL}^{\rm S,I}(+1) = \sigma_{\rm NL}^{\rm S,III}(-1),\ \ \sigma_{\rm NL}^{\rm S,I}(-1) = \sigma_{\rm NL}^{\rm S,III}(+1). \tag{C8}$$

So, the NL conductivities will be identical in both these cases after summing over the nodes. Similarly, when we compare scenario I to II, it can be checked that

$$\begin{aligned}&\sigma_{\rm NL}^{\rm S,I}(+1) = \sigma_{\rm NL}^{\rm S,II}(+1),\ \ \sigma_{\rm NL}^{\rm S,I}(-1) = \sigma_{\rm NL}^{\rm S,II}(-1) \quad \text{for } \mu > 0,\\ &\sigma_{\rm NL}^{\rm S,I}(+1) = \sigma_{\rm NL}^{\rm S,II}(-1),\ \ \sigma_{\rm NL}^{\rm S,I}(-1) = \sigma_{\rm NL}^{\rm S,II}(+1) \quad \text{for } \mu < 0.\end{aligned} \tag{C9}$$

So, in the above two scenarios also, the NL conductivities turned out to be identical after considering the contributions of all the nodes. In conclusion, the NL conductivities do not depend on the position of the Fermi level.

Now, we will present the chiral chemical potential induced NL conductivity. For the TRS preserved Hamiltonian where nodes are separated in energy, Eq. (17) yields

$$\begin{aligned}j_{2,a}^{\delta\mu} = \frac{2e^2\tau}{3\pi^2\hbar^3 v_F}\Big(1-\frac{\tau}{\tau_v}\Big)E_a \\ \times[\mu(\delta\mu^+ + \delta\mu^-) + Q_0(\delta\mu^+ - \delta\mu^-)].\end{aligned} \tag{C10}$$

We emphasize here that the chiral chemical potential is opposite in the nodes with opposite chirality. Thus, the first term which has the addition of chiral chemical potential will vanish. The second term proportional to the energy separation of the nodes will be finite and we obtain

$$\sigma_{abc}^{\delta\mu} = 2\Big(\frac{\tau_v}{\tau}-1\Big)\big(1-r_0^2\big)\tilde{\sigma}_{\rm NL}B_c\delta_{ab}. \tag{C11}$$

[1] X. Wan, A. M. Turner, A. Vishwanath, and S. Y. Savrasov, Topological semimetal and Fermi-arc surface states in the electronic structure of pyrochlore iridates, Phys. Rev. B **83**, 205101 (2011).

[2] H. Weng, C. Fang, Z. Fang, B. A. Bernevig, and X. Dai, Weyl Semimetal Phase in Noncentrosymmetric Transition-Metal Monophosphides, Phys. Rev. X **5**, 011029 (2015).

[3] B. Q. Lv, H. M. Weng, B. B. Fu, X. P. Wang, H. Miao, J. Ma, P. Richard, X. C. Huang, L. X. Zhao, G. F. Chen, Z. Fang, X. Dai, T. Qian, and H. Ding, Experimental Discovery of Weyl Semimetal TaAs, Phys. Rev. X **5**, 031013 (2015).

[4] S.-Y. Xu, I. Belopolski, N. Alidoust, M. Neupane, G. Bian, C. Zhang, R. Sankar, G. Chang, Z. Yuan, C.-C. Lee, S.-M. Huang, H. Zheng, J. Ma, D. S. Sanchez, B. Wang, A. Bansil, F. Chou, P. P. Shibayev, H. Lin, S. Jia *et al.*, Discovery of a Weyl Fermion semimetal and topological Fermi arcs, Science **349**, 613 (2015).

[5] S.-Y. Xu, I. Belopolski, D. S. Sanchez, C. Zhang, G. Chang, C. Guo, G. Bian, Z. Yuan, H. Lu, T.-R. Chang, P. P. Shibayev, M. L. Prokopovych, N. Alidoust, H. Zheng, C.-C. Lee, S.-M. Huang, R. Sankar, F. Chou, C.-H. Hsu, H.-T. Jeng *et al.*, Experimental discovery of a topological Weyl semimetal state in tap, Sci. Adv. **1**, e1501092 (2015).

[6] M. Z. Hasan, S.-Y. Xu, I. Belopolski, and S.-M. Huang, Discovery of Weyl Fermion semimetals and topological Fermi arc states, Annu. Rev. Condens. Matter Phys. **8**, 289 (2017).

[7] B. Yan and C. Felser, Topological materials: Weyl semimetals, Annu. Rev. Condens. Matter Phys. **8**, 337 (2017).

[8] N. P. Armitage, E. J. Mele, and A. Vishwanath, Weyl and Dirac semimetals in three-dimensional solids, Rev. Mod. Phys. **90**, 015001 (2018).

[9] B. Q. Lv, T. Qian, and H. Ding, Experimental perspective on three-dimensional topological semimetals, Rev. Mod. Phys. **93**, 025002 (2021).

[10] A. Thakur, K. Sadhukhan, and A. Agarwal, Dynamic current-current susceptibility in three-dimensional Dirac and Weyl semimetals, Phys. Rev. B **97**, 035403 (2018).

[11] K. Sonowal, A. Singh, and A. Agarwal, Giant optical activity and Kerr effect in type-I and type-II Weyl semimetals, Phys. Rev. B **100**, 085436 (2019).

[12] M. N. Chernodub, Y. Ferreiros, A. G. Grushin, K. Landsteiner, and M. A. H. Vozmediano, Thermal transport, geometry, and anomalies, Phys. Rep. **977**, 1 (2022).

[13] S. Nishihaya, M. Uchida, Y. Nakazawa, R. Kurihara, K. Akiba, M. Kriener, A. Miyake, Y. Taguchi, M. Tokunaga, and M. Kawasaki, Quantized surface transport in topological Dirac semimetal films, Nat. Commun. **10**, 2564 (2019).

[14] S. Nishihaya, M. Uchida, Y. Nakazawa, M. Kriener, Y. Taguchi, and M. Kawasaki, Intrinsic coupling between spatially-separated surface Fermi-arcs in Weyl orbit quantum Hall states, Nat. Commun. **12**, 2572 (2021).

[15] H. Sagayama, D. Uematsu, T. Arima, K. Sugimoto, J. J. Ishikawa, E. O'Farrell, and S. Nakatsuji, Determination of long-range all-in-all-out ordering of Ir^{4+} moments in a pyrochlore iridate $Eu_2Ir_2O_7$ by resonant x-ray diffraction, Phys. Rev. B **87**, 100403(R) (2013).

[16] S. M. Disseler, Direct evidence for the all-in/all-out magnetic structure in the pyrochlore iridates from muon spin relaxation, Phys. Rev. B **89**, 140413(R) (2014).

[17] Z. Wang, H. Weng, Q. Wu, X. Dai, and Z. Fang, Three-dimensional Dirac semimetal and quantum transport in Cd_3As_2, Phys. Rev. B **88**, 125427 (2013).

[18] Z. Wang, Y. Sun, X.-Q. Chen, C. Franchini, G. Xu, H. Weng, X. Dai, and Z. Fang, Dirac semimetal and topological phase transitions in A_3Bi (a = Na, K, Rb), Phys. Rev. B **85**, 195320 (2012).

[19] S.-M. Huang, S.-Y. Xu, I. Belopolski, C.-C. Lee, G. Chang, B. Wang, N. Alidoust, G. Bian, M. Neupane, C. Zhang, S. Jia, A. Bansil, H. Lin, and M. Z. Hasan, A Weyl Fermion semimetal with surface Fermi arcs in the transition metal monopnictide TaAs class, Nat. Commun. **6**, 7373 (2015).

[20] A. A. Zyuzin, S. Wu, and A. A. Burkov, Weyl semimetal with broken time reversal and inversion symmetries, Phys. Rev. B **85**, 165110 (2012).

[21] G. Chang, B. Singh, S.-Y. Xu, G. Bian, S.-M. Huang, C.-H. Hsu, I. Belopolski, N. Alidoust, D. S. Sanchez, H. Zheng, H. Lu, X. Zhang, Y. Bian, T.-R. Chang, H.-T. Jeng, A. Bansil, H. Hsu, S. Jia, T. Neupert, H. Lin *et al.*, Magnetic and noncentrosymmetric Weyl Fermion semimetals in the RAlGe family of compounds (R = rare earth), Phys. Rev. B **97**, 041104(R) (2018).

[22] H.-Y. Yang, B. Singh, J. Gaudet, B. Lu, C.-Y. Huang, W.-C. Chiu, S.-M. Huang, B. Wang, F. Bahrami, B. Xu, J. Franklin, I. Sochnikov, D. E. Graf, G. Xu, Y. Zhao, C. M. Hoffman, H. Lin, D. H. Torchinsky, C. L. Broholm, A. Bansil *et al.*, Noncollinear ferromagnetic Weyl semimetal with anisotropic anomalous Hall effect, Phys. Rev. B **103**, 115143 (2021).

[23] R. Boyd, *Nonlinear Optics* (Academic, Amsterdam, 2008).

[24] J. Orenstein, J.E. Moore, T. Morimoto, D.H. Torchinsky, J.W. Harter, and D. Hsieh, Topology and symmetry of quantum materials via nonlinear optical responses, Annu. Rev. Condens. Matter Phys. **12**, 247 (2021).

[25] S. K. Das, T. Nag, and S. Nandy, Topological Magnus responses in two- and three-dimensional systems, Phys. Rev. B **104**, 115420 (2021).

[26] C.-K. Chan, N. H. Lindner, G. Refael, and P. A. Lee, Photocurrents in Weyl semimetals, Phys. Rev. B **95**, 041104(R) (2017).

[27] F. de Juan, A. G. Grushin, T. Morimoto, and J. E. Moore, Quantized circular photogalvanic effect in Weyl semimetals, Nat. Commun. **8**, 15995 (2017).

[28] L. E. Golub, E. L. Ivchenko, and B. Z. Spivak, Photocurrent in gyrotropic Weyl semimetals, JETP Lett. **105**, 782 (2017).

[29] D. E. Kharzeev, Y. Kikuchi, R. Meyer, and Y. Tanizaki, Giant photocurrent in asymmetric Weyl semimetals from the helical magnetic effect, Phys. Rev. B **98**, 014305 (2018).

[30] L. E. Golub and E. L. Ivchenko, Circular and magnetoinduced photocurrents in Weyl semimetals, Phys. Rev. B **98**, 075305 (2018).

[31] D. E. Parker, T. Morimoto, J. Orenstein, and J. E. Moore, Diagrammatic approach to nonlinear optical response with application to Weyl semimetals, Phys. Rev. B **99**, 045121 (2019).

[32] B. Sadhukhan and T. Nag, Role of time reversal symmetry and tilting in circular photogalvanic responses, Phys. Rev. B **103**, 144308 (2021).

[33] B. Sadhukhan and T. Nag, Electronic structure and unconventional nonlinear response in double Weyl semimetal $SrSi_2$, Phys. Rev. B **104**, 245122 (2021).

[34] J. Li, T. Xu, G.-B. Zhu, and H. Pan, Photoinduced anomalous Hall and nonlinear Hall effect in borophene, Solid State Commun. **322**, 114092 (2020).

[35] E. Deyo, L. E. Golub, E. L. Ivchenko, and B. Spivak, Semiclassical theory of the photogalvanic effect in non-centrosymmetric systems, arXiv:0904.1917.

[36] J. E. Moore and J. Orenstein, Confinement-Induced Berry Phase and Helicity-Dependent Photocurrents, Phys. Rev. Lett. **105**, 026805 (2010).

[37] I. Sodemann and L. Fu, Quantum Nonlinear Hall Effect Induced by Berry Curvature Dipole in Time-Reversal Invariant Materials, Phys. Rev. Lett. **115**, 216806 (2015).

[38] Q. Ma, S.-Y. Xu, H. Shen, D. MacNeill, V. Fatemi, T.-R. Chang, A. M. Mier Valdivia, S. Wu, Z. Du, C.-H. Hsu, S. Fang, Q. D. Gibson, K. Watanabe, T. Taniguchi, R. J. Cava, E. Kaxiras, H.-Z. Lu, H. Lin, L. Fu, N. Gedik *et al.*, Observation of the nonlinear Hall effect under time-reversal-symmetric conditions, Nature (London) **565**, 337 (2019).

[39] Z. Z. Du, H.-Z. Lu, and X. C. Xie, Nonlinear Hall effects, Nat. Rev. Phys. **3**, 744 (2021).

[40] C. Ortix, Nonlinear Hall effect with time-reversal symmetry: Theory and material realizations, Adv. Quantum Technol. **4**, 2100056 (2021).

[41] E. J. König, H.-Y. Xie, D. A. Pesin, and A. Levchenko, Photogalvanic effect in Weyl semimetals, Phys. Rev. B **96**, 075123 (2017).

[42] H. Rostami and M. Polini, Nonlinear anomalous photocurrents in Weyl semimetals, Phys. Rev. B **97**, 195151 (2018).

[43] C. Zeng, S. Nandy, and S. Tewari, Nonlinear transport in Weyl semimetals induced by Berry curvature dipole, Phys. Rev. B **103**, 245119 (2021).

[44] A. Cortijo, Magnetic-field-induced nonlinear optical responses in inversion symmetric Dirac semimetals, Phys. Rev. B **94**, 235123 (2016).

[45] T. Morimoto, S. Zhong, J. Orenstein, and J. E. Moore, Semiclassical theory of nonlinear magneto-optical responses with applications to topological Dirac/Weyl semimetals, Phys. Rev. B **94**, 245121 (2016).

[46] S. Nandy, C. Zeng, and S. Tewari, Chiral anomaly induced nonlinear Hall effect in multi-Weyl semimetals, Phys. Rev. B **104**, 205124 (2021).

[47] Y. Gao, Semiclassical dynamics and nonlinear charge current, Front. Phys. **14**, 33404 (2019).

[48] E. V. Gorbar, V. A. Miransky, I. A. Shovkovy, and P. O. Sukhachov, Second-order chiral kinetic theory: Chiral magnetic and pseudomagnetic waves, Phys. Rev. B **95**, 205141 (2017).

[49] L. E. Golub, E. L. Ivchenko, and B. Spivak, Semiclassical theory of the circular photogalvanic effect in gyrotropic systems, Phys. Rev. B **102**, 085202 (2020).

[50] V. A. Zyuzin, Chiral electric separation effect in Weyl semimetals, Phys. Rev. B **98**, 165205 (2018).

[51] A. A. Zyuzin, M. Silaev, and V. A. Zyuzin, Nonlinear chiral transport in Dirac semimetals, Phys. Rev. B **98**, 205149 (2018).

[52] R.-H. Li, O. G. Heinonen, A. A. Burkov, and S. S.-L. Zhang, Nonlinear Hall effect in Weyl semimetals induced by chiral anomaly, Phys. Rev. B **103**, 045105 (2021).

[53] P. He, S. S.-L. Zhang, D. Zhu, S. Shi, O. G. Heinonen, G. Vignale, and H. Yang, Nonlinear Planar Hall Effect, Phys. Rev. Lett. **123**, 016801 (2019).

[54] G. Pacchioni, The Hall effect goes nonlinear, Nat. Rev. Mater. **4**, 514 (2019).

[55] K. Kang, T. Li, E. Sohn, J. Shan, and K. F. Mak, Nonlinear anomalous Hall effect in few-layer WTe_2, Nat. Mater. **18**, 324 (2019).

[56] O. O. Shvetsov, V. D. Esin, A. V. Timonina, N. N. Kolesnikov, and E. V. Deviatov, Nonlinear Hall effect in three-dimensional Weyl and Dirac semimetals, JETP Lett. **109**, 715 (2019).

[57] M.-C. Chang and Q. Niu, Berry Phase, Hyperorbits, and the Hofstadter Spectrum, Phys. Rev. Lett. **75**, 1348 (1995).

[58] G. Sundaram and Q. Niu, Wave-packet dynamics in slowly perturbed crystals: Gradient corrections and Berry-phase effects, Phys. Rev. B **59**, 14915 (1999).

[59] Y. Gao, S. A. Yang, and Q. Niu, Field Induced Positional Shift of Bloch Electrons and Its Dynamical Implications, Phys. Rev. Lett. **112**, 166601 (2014).

[60] Y. Gao, S. A. Yang, and Q. Niu, Geometrical effects in orbital magnetic susceptibility, Phys. Rev. B **91**, 214405 (2015).

[61] K. Das, S. K. Singh, and A. Agarwal, Chiral anomalies induced transport in Weyl metals in quantizing magnetic field, Phys. Rev. Research **2**, 033511 (2020).

[62] T. Morimoto and N. Nagaosa, Scaling laws for nonlinear electromagnetic responses of Dirac Fermion, Phys. Rev. B **93**, 125125 (2016).

[63] S. Das, K. Das, and A. Agarwal, Nonlinear magnetoconductivity in Weyl and multi-Weyl semimetals in quantizing magnetic field, Phys. Rev. B **105**, 235408 (2022).

[64] K. Das and A. Agarwal, Intrinsic Hall conductivities induced by the orbital magnetic moment, Phys. Rev. B **103**, 125432 (2021).

[65] K. Das and A. Agarwal, Linear magnetochiral transport in tilted type-I and type-II Weyl semimetals, Phys. Rev. B **99**, 085405 (2019).

[66] H. B. Nielsen and M. Ninomiya, The Adler-Bell-Jackiw anomaly and Weyl Fermions in a crystal, Phys. Lett. B **130**, 389 (1983).

[67] S. Murakami, Phase transition between the quantum spin Hall and insulator phases in 3d: Emergence of a topological gapless phase, New J. Phys. **9**, 356 (2007).

[68] I. Belopolski, P. Yu, D. S. Sanchez, Y. Ishida, T.-R. Chang, S. S. Zhang, S.-Y. Xu, H. Zheng, G. Chang, G. Bian, H.-T. Jeng, T. Kondo, H. Lin, Z. Liu, S. Shin, and M. Z. Hasan, Signatures of a time-reversal symmetric Weyl semimetal with only four Weyl points, Nat. Commun. **8**, 942 (2017).

[69] M. M. Vazifeh and M. Franz, Electromagnetic Response of Weyl Semimetals, Phys. Rev. Lett. **111**, 027201 (2013).

[70] H.-R. Chang, J. Zhou, S.-X. Wang, W.-Y. Shan, and D. Xiao, Rkky interaction of magnetic impurities in Dirac and Weyl semimetals, Phys. Rev. B **92**, 241103(R) (2015).

[71] C. J. Tabert, J. P. Carbotte, and E. J. Nicol, Optical and transport properties in three-dimensional Dirac and Weyl semimetals, Phys. Rev. B **93**, 085426 (2016).

[72] S. P. Mukherjee and J. P. Carbotte, Anomalous DC Hall response in noncentrosymmetric tilted Weyl semimetals, J. Phys.: Condens. Matter **30**, 115702 (2018).

[73] J. I. Facio, D. Efremov, K. Koepernik, J.-S. You, I. Sodemann, and J. van den Brink, Strongly Enhanced Berry Dipole at Topological Phase Transitions in BiTeI, Phys. Rev. Lett. **121**, 246403 (2018).

[74] O. Matsyshyn and I. Sodemann, Nonlinear Hall Acceleration and the Quantum Rectification Sum Rule, Phys. Rev. Lett. **123**, 246602 (2019).

[75] N. W. Ashcroft and N. D. Mermin, *Solid State Physics*, HRW international editions (Holt, Rinehart and Winston, New York, 1976).

[76] K.-S. Kim, H.-J. Kim, and M. Sasaki, Boltzmann equation approach to anomalous transport in a Weyl metal, Phys. Rev. B **89**, 195137 (2014).

[77] E. L. Ivchenko and G. E. Pikus, New photogalvanic effect in gyrotropic crystals, ZhETF Pisma Redaktsiiu **27**, 640 (1978) [Sov. J. Exp. Theor. Phys. Lett. **27**, 604 (1978)].

[78] V. V. Bel'kov, S. D. Ganichev, E. L. Ivchenko, S. A. Tarasenko, W. Weber, S. Giglberger, M. Olteanu, H.-P. Tranitz, S. N. Danilov, P. Schneider, W. Wegscheider, D. Weiss, and W. Prettl, Magneto-gyrotropic photogalvanic effects in semiconductor quantum wells, J. Phys.: Condens. Matter **17**, 3405 (2005).

[79] E. L. Ivchenko and S. D. Ganichev, Spin-photogalvanics, in *Spin Physics in Semiconductors*, edited by M. I. Dyakonov (Springer, Berlin, 2008), pp. 245.

[80] V. V. Belkov and S. D. Ganichev, Magneto-gyrotropic effects in semiconductor quantum wells, Semicond. Sci. Technol. **23**, 114003 (2008).

[81] G. L. J. A. Rikken, J. Fölling, and P. Wyder, Electrical Magnetochiral Anisotropy, Phys. Rev. Lett. **87**, 236602 (2001).

[82] G. L. J. A. Rikken and P. Wyder, Magnetoelectric Anisotropy in Diffusive Transport, Phys. Rev. Lett. **94**, 016601 (2005).

[83] E. L. Ivchenko and B. Spivak, Chirality effects in carbon nanotubes, Phys. Rev. B **66**, 155404 (2002).

[84] B. Spivak and A. Zyuzin, Signature of the electron-electron interaction in the magnetic-field dependence of nonlinear *i-v* characteristics in mesoscopic systems, Phys. Rev. Lett. **93**, 226801 (2004).

[85] A. Sekine, D. Culcer, and A. H. MacDonald, Quantum kinetic theory of the chiral anomaly, Phys. Rev. B **96**, 235134 (2017).

[86] A. Sekine and N. Nagaosa, Quantum kinetic theory of thermoelectric and thermal transport in a magnetic field, Phys. Rev. B **101**, 155204 (2020).

[87] P. Bhalla, K. Das, D. Culcer, and A. Agarwal, Quantum geometry induced second harmonic generation, arXiv:2108.04082.

[88] R. B. Atencia, Q. Niu, and D. Culcer, Semiclassical response of disordered conductors: Extrinsic carrier velocity and spin and field-corrected collision integral, Phys. Rev. Research **4**, 013001 (2022).

[89] C. M. Hurd, *The Hall Effect in Metals and Alloys* (Plenum, New York, 1972).

[90] K. Das and A. Agarwal, Berry curvature induced thermopower in type-I and type-II Weyl semimetals, Phys. Rev. B **100**, 085406 (2019).

[91] J. M. Ziman, *Principles of the Theory of Solids* (Cambridge University Press, Cambridge, 1972).